



ORIGINAL ARTICLE

Delta-6 desaturase FADS2 is a tumor-promoting factor in cholangiocarcinoma

Kohsei Hasegawa^{1,2,3} | Haruna Fujimori¹  | Kohta Nakatani⁴ | Masatomo Takahashi⁴ | Yoshihiro Izumi⁴ | Takeshi Bamba⁴ | Mao Nakamura-Shima¹ | Rie Shibuya-Takahashi¹ | Mai Mochizuki¹ | Yuta Wakui⁵ | Makoto Abue⁵ | Wataru Iwai⁵ | Daisuke Fukushi⁶ | Kennichi Satoh⁶ | Kazunori Yamaguchi⁷ | Norihisa Shindo⁸ | Jun Yasuda⁷ | Naoki Asano^{1,9} | Takayuki Imai² | Yukinori Asada² | Yukio Katori³ | Keiichi Tamai¹ 

¹Division of Cancer Stem Cell, Miyagi Cancer Center Research Institute, Natori, Miyagi, Japan

²Department of Head and Neck Surgery, Miyagi Cancer Center, Natori, Miyagi, Japan

³Department of Otolaryngology-Head and Neck Surgery, Tohoku University Graduate School of Medicine, Sendai, Miyagi, Japan

⁴Division of Metabolomics, Medical Research Center for High Depth Omics, Medical Institute of Bioregulation, Kyushu University, Fukuoka, Japan

⁵Division of Gastroenterology, Miyagi Cancer Center, Natori, Miyagi, Japan

⁶Division of Gastroenterology, Tohoku Medical and Pharmaceutical University, Sendai, Miyagi, Japan

⁷Division of Molecular and Cellular Oncology, Miyagi Cancer Center Research Institute, Natori, Miyagi, Japan

⁸Division of Cancer Chromosome Biology Unit, Miyagi Cancer Center Research Institute, Natori, Miyagi, Japan

⁹Division of Gastroenterology, Tohoku University Graduate School of Medicine, Sendai, Japan

Correspondence

Haruna Fujimori, Division of Cancer Stem Cell, Miyagi Cancer Center Research Institute, 47-1, Medeshima-Shiote, Natori, Miyagi, 981-1293, Japan.
Email: fuji.spr.na@gmail.com

Funding information

Takeda Medical Research Foundation; Kobayashi Foundation for Cancer Research; Japan Agency for Medical Research and Development, Grant/Award Number: JP22ama121055; Japan Society for the Promotion of Science, Grant/Award Number: 19K08430, 20K09701, 21H02396, 21K07137, 21K07186, 21K07973, 22K07974, 22K08085, 22K09678 and 22K09696; MEXT Cooperative Research Project Program, Medical Research Center Initiative for High Depth Omics, and CURE, Grant/Award Number: JPMXP1323015486

Abstract

Cholangiocarcinoma is a fatal disease with limited therapeutic options. We screened genes required for cholangiocarcinoma tumorigenicity and identified FADS2, a delta-6 desaturase. FADS2 depletion reduced in vivo tumorigenicity and cell proliferation. In clinical samples, FADS2 was expressed in cancer cells but not in stromal cells. FADS2 inhibition also reduced the migration and sphere-forming ability of cells and increased apoptotic cell death and ferroptosis markers. Lipidome assay revealed that triglyceride and cholesterol ester levels were decreased in FADS2-knockdown cells. The oxygen consumption ratio was also decreased in FADS2-depleted cells. These data indicate that FADS2 depletion causes a reduction in lipid levels, resulting in decrease of energy production and attenuation of cancer cell malignancy.

KEYWORDS

cholangiocarcinoma, cholesterol esters, delta-6 desaturase, FADS2, triglyceride

Abbreviations: BSA, bovine serum albumin; CCA, cholangiocarcinoma; ELOVL2, elongation of very-long-chain fatty acids protein 2; FA, fatty acid; FADS2, fatty acid desaturase 2; FBS, fetal bovine serum; GSH, glutathione; GSSG, oxidized glutathione; PDX, patient-derived xenograft; SCD1, stearoyl-CoA desaturase 1

Kohsei Hasegawa and Haruna Fujimori contributed equally to this work.

This is an open access article under the terms of the [Creative Commons Attribution-NonCommercial](https://creativecommons.org/licenses/by-nc/4.0/) License, which permits use, distribution and reproduction in any medium, provided the original work is properly cited and is not used for commercial purposes.

© 2024 The Author(s). *Cancer Science* published by John Wiley & Sons Australia, Ltd on behalf of Japanese Cancer Association.

1 | INTRODUCTION

Cholangiocarcinoma (CCA) is a disease entity that comprises diverse epithelial tumors with features of cholangiocyte differentiation.¹ CCA is difficult to treat and has an incidence of <6 cases per 100,000 people² and the mortality rate is 1 per 100,000 people worldwide.³ Most patients are diagnosed at an advanced stage, and there are consequently few therapeutic options, including targeted therapies.

Cholangiocarcinoma tumor tissues consist of heterogeneous cell populations,² comprising a mixture of highly and minimally malignant cells. This heterogeneity involves several cell characteristics, including chemoresistance, stemness, and tumorigenicity.⁴ Patient-derived xenografts (PDX) in mice are an appropriate experimental model for reproducing tumor heterogeneity in the tumor micro-environment.^{5,6} The xenografted tissue is similar to the original human cancerous tissue⁷ and is widely used in preclinical research.⁸ Proliferating xenografted cancer cells originate from a highly tumorigenic subpopulation, which is enriched in serially transplanted xenografts in mice.⁹ Thus, highly tumorigenic, therapy-resistant cells can be identified using this model.

Fatty acids (FAs) consist of a terminal carboxyl group and a hydrocarbon chain, mostly with an even number of carbon atoms that can be either saturated or unsaturated.¹⁰ Unsaturated lipids are produced by FA desaturases, such as SCD1 and FADS2. Alterations in FA metabolism have been increasingly reported in cancer cells. Unsaturated lipids are increased in ovarian cancer stem cells.¹¹ The expression of SCD1 and FADS2 are increased in metastatic tumors, and SCD1/FADS2 inhibitors in combination with cisplatin synergistically repress tumor cell dissemination.¹² In glioblastoma, ELOVL2, which is a key polyunsaturated FA synthesis enzyme, is upregulated in cancer stem cells through EGFR signaling.¹³ However, little is known regarding unsaturated enzyme-dependent mechanisms, especially in CCA.

In this study, we aimed to identify a gene required for tumorigenicity using a xenograft model, which led to the identification of the delta-6 desaturase FADS2.

2 | MATERIALS AND METHODS

2.1 | Ethics statements

This study was conducted in accordance with the principles of the Declaration of Helsinki and approved by the ethics committee of the Miyagi Cancer Center Research Institute (Natori, Japan). The animal experimental protocols were approved by the Miyagi Cancer Center Animal Care and Use Committee (permit number AE.22.01).

2.2 | Cell lines

The CCA PDX cell line, CHOL1, was established using serial xenografts of tumor tissues derived from a human CCA patient with

written informed consent (50-year-old male), as described previously.¹⁴ TFK-1 cells were provided by the Cell Resource Center for Biomedical Research, Institute of Development, Aging, and Cancer, Tohoku University. Both cell lines were maintained in RPMI medium supplemented with 10% FBS.

2.3 | Quantitative real-time PCR

Total RNA was extracted from cells using the RNeasy Mini Kit (Qiagen), reverse transcribed using a PrimeScript II cDNA Synthesis Kit (Takara Bio) and then real-time PCR was performed using the Brilliant III Ultra-Fast SYBR Green QPCR Master Mix (Agilent Technologies). β -Actin was used as the housekeeping gene, and data were analyzed using the $\Delta\Delta C_t$ method. The primer sequences were as follows: β -Actin forward primer 5'-ccaaccgcgagaagatga-3', β -actin reverse primer 5'-tccatcacgatgccagt-3', FADS2 forward primer 5'-ttcagtgacacacctaactcc, and FADS2 reverse primer 5'-cacatagagacttcaccgcg.

2.4 | Cell proliferation assay

Cells were plated in 96-well plates, and the relative cell number was determined by image analysis using an Incucyte Zoom device (Sartorius) or by MTT assay. For the MTT assay, MTT (5 mg/mL, 1:10) was added to the medium, and after 2 h, an equal volume of 10% sodium dodecyl sulfate (SDS) in 0.01 M HCl was added, and further incubated overnight, after which the absorbance at 550 nm was measured.¹⁵

2.5 | Sphere-formation assay

On day 0, 1×10^4 cells were plated in DMEM/F12 (Fujifilm Wako Pure Chemical Corporation) supplemented with B27 (1:50; Thermo Fisher Scientific), epidermal growth factor (20 ng/mL; PeproTech), and fibroblast growth factor-2 (20 ng/mL; PeproTech) in 96-well Nunclon Sphera plates (Thermo Fisher Scientific). For FADS2 knock-down, small interfering RNA (siRNA) was transfected on day 0, as described below. On day 6, MTT (5 mg/mL, 1:10) was added to the medium, and after 2 h, an equal volume of 10% SDS in 0.01 M HCl was added and further incubated overnight, after which the absorbance at 550 nm was measured.¹⁵

2.6 | Small interfering RNA

Negative control siRNA (12935-300), FADS2 siRNAs FADS2#23 (s18023), FADS2#24 (s18024), and FADS2#25 (s18025) were purchased from Thermo Fisher Scientific. siRNA transfection was performed using lipofectamine RNAiMAX Reagent (Life Technologies).¹⁶

2.7 | In vivo tumorigenesis assay

Tumor formation was assayed as previously described.¹⁷ Briefly, the cells were suspended in 50 μ L of phosphate-buffered saline (PBS) and an equal volume of Matrigel matrix (BD Biosciences) on ice and then injected into immunodeficient NOD/Shi-scid, IL-2R γ null (NOG) mice using a 1-mL syringe. Tumor formation was monitored weekly, and the tumor volumes were calculated using the following formula: $1/2 (\text{length} \times \text{width}^2)$.

2.8 | Apoptosis assay

For flow cytometry, cells were harvested using 0.25% trypsin. The cells were resuspended in annexin-binding buffer (BioLegend) and stained with FITC-conjugated annexin V (BioLegend) and propidium iodide. After incubation for 15 min, the cells were analyzed using an SA3800 spectral flow cytometer (SONY). For the luminescence assay, caspase-Glo 3/7 (Promega) was used according to the manufacturer's protocol.

2.9 | Scratch assay

The scratch-wound assay was performed as described previously.¹⁸ Cells were seeded in 24-well plates in medium containing 3% FBS, incubated until confluent, and then treated with 2.5 μ g/mL mitomycin C (Fujifilm-Wako) for 4 h. A yellow pipette tip was used to create straight scratch wounds in the cell monolayer. The medium was replaced with serum-free medium, and after 24 h of incubation, the area occupied by cells that had migrated into the scratch wound area was measured using ImageJ software. To inhibit FADS2, SC26196 (Cayman Chemical) was added to the medium 3 days before scratching.

2.10 | Western blot analysis

Western blotting was performed as previously described, with minor modifications.¹⁵ Cells were washed once with Dulbecco's PBS or plain medium, suspended in SDS-loading buffer (100 mM Tris-Cl pH 6.8, 4% SDS, 0.2% bromophenol blue, 20% glycerol, and 2% β -mercaptoethanol), sonicated for 5 min, heated to 100°C for 5 min, and then subjected to SDS-PAGE. The separated proteins were transferred onto an Immobilon-P Membrane (Bio-Rad) and blocked with 2% BSA in Tris-buffered saline containing 0.1% Tween® 20 (TTBS) for 30 min at room temperature. The membrane was then incubated with primary antibody, washed, and incubated with secondary antibody. Primary antibody binding was detected using Clarity Western ECL Substrate (Bio-Rad) and images were captured using a

FUSION-SOLO.7S.EDGE imaging system (Vilber Bio Imaging). The antibodies used in this study were anti-glutathione peroxidase 4 (AB125066, Abcam), anti-pan-Akt (C67E7, rabbit mAb #4691, Cell Signaling Technology), and anti-phospho-AKT (Ser473) (#4069, Cell Signaling Technology).

2.11 | In situ hybridization

A CCA tissue-array (#GA802a) was purchased from TissueArray Co. FADS2 mRNA in the tissue microarray was detected by RNAscope 2.5 HD Assay-BROWN assay (Advanced Cell Diagnostics) according to the manufacturer's protocol. The probes used were Hs-FADS2 (#569811; Advanced Cell Diagnostics), a positive control probe (Hs-PP1B #313901), and a negative control probe (dapB #310043).

2.12 | Microarray analysis

Expression profiling of xenografted tumors and FADS2-knockdown cells was performed using a microarray (SurePrint G3 8 \times 60k, Agilent).¹⁵ Data processing was performed using R statistical software (version 4.2.0),¹⁹ and GSEA was performed as described previously.²⁰ A time-series analysis was conducted using maSigPro.²¹

2.13 | Quantification of the glutathione/oxidized glutathione (GSH/GSSG) ratio

Detection and quantification of total glutathione (GSH + GSSG), GSSG, and GSH/GSSG ratios were performed using the GSH/GSSG-Glo assay (Promega). Cells were cultured and treated in white assay plates (SPL). The media were discarded and replaced with either total GSH lysis reagent or GSSG lysis reagent, and the cells were agitated for 5 min. Both plates were kept at room temperature for 30 min before luciferin generation reagent was added. The plates were briefly agitated on an orbital shaker and allowed to equilibrate at room temperature for 15 min. The luminescence was measured using a Synergy LX plate reader (Agilent), and the GSH/GSSG ratio was calculated according to the manufacturer's guidelines.

2.14 | Quantification of intracellular lipid droplets

Cells were treated with siRNA or SC26196. After 2 days (CHOL1) or 3 days (TFK-1), cells were stained with Lipi-Green (1:1000, Dojindo) for 1 h at 37°C. The cells were then trypsinized, and the Lipi-Green intensity was measured by flow cytometry (SA3800, SONY). Images were obtained using a fluorescence microscope (IX73; EVIDENT).

2.15 | Flux analyzer assay

The oxygen consumption ratio was measured using a flux analyzer (Seahorse XF96, Agilent).²² CHOL1 and TFK-1 cells were plated on Seahorse XFe96 V3 PS plates. The cells were cultured under standard 5% CO₂ and 37°C conditions. Seahorse XF base medium enriched with 10mM glucose, 2mM L-glutamine, and 1mM sodium pyruvate was equilibrated to 37°C and an adjusted pH of 7.35 ± 0.05. All wells were carefully washed three times with the Seahorse XF base medium and then incubated for 1 h in assay medium in a 37°C CO₂-free incubator before the measurement. Values were normalized to the relative cell number measured using an Incucyte device (Sartorius). Basal respiration was measured at the time point without the mitochondria inhibitor treatment. Maximal respiration was measured at the time point after the carbonyl cyanide 4-(trifluoromethoxy) phenylhydrazone (FCCP, Sigma Aldrich), a potent uncoupler of mitochondrial oxidative phosphorylation, treatment.

2.16 | Gas chromatography-mass spectrometry (GC-MS)

Gas chromatography-mass spectrometry analysis was performed at Shimadzu Techno-Research. Briefly, CHOL1 cells were harvested and sonicated on ice. Lipids were extracted from the lysate with chloroform/methanol. The extracted organic layer was evaporated to dryness, followed by methyl esterification with 4% methanolic HCl at 90°C for 2 h. After quenching with distilled water, palmitic acid-d₃₁ was added as an internal standard (IS). The ISs and the resulting FA methyl esters were extracted with *n*-hexane. The extracted *n*-hexane layer was analyzed by GC-MS (GCMS-QP2020, Shimadzu). TC-70 column (60m × 0.25mm i.d., 0.25µm film thickness; GL Sciences) was used for the analysis.

2.17 | Lipidomic analysis

CHOL1 cell samples (approximately 2.3 × 10⁵ cells) were prepared for extracting lipids using the Bligh and Dyer method²³ with minor modifications.²⁴ Briefly, the CHOL1 cells were washed twice with 10mL of PBS and quenched with 1mL of ice-cold methanol. After scraping, the cell suspension (~1mL) was transferred into a 2-mL Eppendorf tube and mixed with 10µL of IS solution A (Mouse SPLASH Lipidomix Mass Spec Standard, Avanti Polar Lipids Inc.) containing phosphatidylcholine (PC) 15:0/[²H₇]18:1 (1.0nmol), phosphatidylethanolamine (PE) 15:0/[²H₇]18:1 (0.070nmol), phosphatidylserine (PS) 15:0/[²H₇]18:1 (0.20nmol), phosphatidylglycerol (PG) 15:0/[²H₇]18:1 (0.050nmol), phosphatidylinositol (PI) 15:0/[²H₇]18:1 (0.20nmol), phosphatidic acid (PA) 15:0/[²H₇]18:1 (0.10nmol), lysophosphatidylcholine (LPC) [²H₇]18:1 (0.45nmol), lysophosphatidylethanolamine (LPE) [²H₇]18:1 (0.020nmol), cholesteryl ester (ChE) [²H₇]18:1 (2.5nmol), diacylglycerol (DG) 15:0/[²H₇]18:1 (0.15nmol), triacylglycerol (TG) 15:0/[²H₇]18:1/15:0

(0.35nmol), and sphingomyelin (SM) d18:1/[²H₉]18:1 (0.20nmol), and 10µL of IS solution B (Avanti Polar Lipids Inc.) containing ceramide (Cer) d[²H₇]18:1/15:0 (0.10nmol), hexosylceramide (HexCer) d[²H₅]18:1/18:1 (0.10nmol), free FA [¹³C₁₆]16:0 (0.10nmol), monoacylglycerol (MG) [²H₇]18:1 (1.0nmol), and [²H₇]cholesterol (3.0nmol). The samples were vigorously mixed by vortexing for 1min followed by 5min of sonication. The samples were centrifuged at 16,000 × g at 4°C for 5min, and the supernatant (400µL) was collected in clean tubes for lipidomic analysis. After mixing with 400µL of chloroform and 360µL of water, phase separation of aqueous and organic layers was performed via centrifugation (16,000 × g, 4°C, 5min). The organic layer (bottom, 280µL) obtained by phase separation was dried under a nitrogen stream and stored at -80°C until analysis. Prior to lipidomic analysis, the dried sample was reconstituted in methanol/chloroform (1/1, v/v, 100µL).

The analytical conditions for lipidomics using supercritical fluid chromatography-tandem mass spectrometry (SFC-MS/MS) were performed as previously described.^{24,25} The SFC (Nexera UC system, Shimadzu Co.) conditions were as follows: an ACQUITY UPC² Torus DEA column (3.0mm i.d. × 100mm, 1.7µm particle size, Waters); injection volume, 1µL; column temperature, 50°C; mobile phase A, supercritical carbon dioxide; mobile phase B (modifier) and make-up pump solvent; methanol/water (95/5, v/v) with 0.1% (w/v) ammonium acetate; flow rate of mobile phase, 1.0mL/min; flow rate of make-up pump, 0.1mL/min; and back pressure regulator, 10MPa. The gradient conditions were as follows: 1% B, 0–1min; 1–75% B, 1–24min; 75% B, 24–26min; and 1% B, 26–30min. The triple quadrupole mass spectrometry (TQMS, LCMS-8060NX, Shimadzu Co.) analysis conditions were as follows: polarity, positive and negative ionization; electrospray voltage, 4kV in the positive ion mode and -3.5kV in the negative ion mode; nebulizer gas flow rate, 3.0L/min; drying gas flow rate, 10.0L/min; desolvation line temperature, 250°C; heat block temperature, 400°C; and detector voltage, 2.16kV. The multiple reaction monitoring (MRM) parameters per one time period were as follows: limit on number of MRM transitions, 150; dwell time, 2ms; pause time, 2ms; and polarity switching time, 5ms. The analytical platform for lipidomic analysis was controlled using LabSolutions (version 5.99 SP2, Shimadzu Co.), and data analysis was performed using Multi-ChromatoAnalysT (Beforce).

2.18 | Fluorescence recovery after photobleaching (FRAP) analysis

The specific methods are described in the Supporting Information (Data S1).

2.19 | Reactive oxygen species (ROS) generation

The specific methods are described in the Supporting Information (Data S1).

2.20 | Statistical analysis

The statistical analyses were performed using GraphPad Prism version 10.0.2 (GraphPad Software). Differences between two groups were analyzed using an unpaired *t*-test. One-way ANOVA tests were used for three or more groups. **p* < 0.05, ***p* < 0.01, ****p* < 0.001, and *****p* < 0.0001 were considered to indicate statistical significance. All data were expressed as means ± the SEM and represent the results of three independent experiments.

3 | RESULTS

3.1 | FADS2 is required for CCA tumorigenesis

To identify genes required for tumorigenicity, we investigated serially transplanted xenografts in immunodeficient mice, which were enriched in a subset of the cell population that possesses tumor reconstruction activity. Patient-derived human CCA cells (CHOL1) were subcutaneously implanted into NOG mice and serially passaged into new mice as previously described (Figure 1A), resulting in shorter passage intervals for each generation. Tumor samples were collected at each passage, and an expression microarray was performed. A time-series analysis revealed clusters with an upward trend. We selected genes in clusters that were not previously reported to be associated with CCA. We focused on *FADS2* because *FADS2* mRNA expression increased with serial passaging (Figure 1B). *FADS2* knockdown in CHOL1 and TFK-1 cells (Figure 1C) suppressed tumor development in NOG mice (Figure 1D,E). In vitro proliferation capability was also decreased under the treatment of *FADS2* knockdown in both two cell lines (Figure 1F). We examined the *FADS2* expression in human CCA specimens. Because no anti-*FADS2* antibody was available for immunohistochemistry, we performed in situ hybridization of *FADS2* mRNA in FFPE human CCA specimens. *FADS2* mRNA was observed in CCA tumor cells but not in the stroma (Figure 1G). These data suggest that *FADS2* is required for tumorigenesis.

3.2 | FADS2 inhibitor attenuated cancer cell malignancy

SC26196 is a well-known *FADS2* inhibitor.²⁶ Next, we confirmed that inhibition of *FADS2* by SC26196 reduced cell proliferation in both two cell lines (Figure 2A). AKT signaling is known to be involved in cell proliferation.²⁷ We found that inhibition of *FADS2* reduced AKT phosphorylation under the 2-μM SC26196 treatment in both CCA cell lines (Figure 2B).

We performed a sphere-formation assay, which is known to reflect stemness characteristics.²⁸ Treatment of CHOL1 cells with the *FADS2* inhibitor SC26196 (2 μM) reduced their sphere-forming ability by 34.8% compared with controls (Figure 2C). Similar results were obtained in TFK-1 cells (Figure 2C).

Migration activity is one of the hallmarks of cancer.²⁹ To test the cell migration activity following *FADS2* inhibitor treatment, we performed a scratch assay. Treatment with the *FADS2* inhibitor reduced the migration capacity by 24% in CHOL1 cells and 50% in TFK-1 cells (Figure 2D).

3.3 | Inhibition of FADS2 promoted apoptosis and ferroptosis

Cell death is a factor that determines cancer cell viability, resulting in tumorigenicity. Therefore, we tested whether *FADS2* is involved in apoptosis. The early and late apoptotic rates of the two cell lines were increased by *FADS2* inhibition (Figure 3A). We measured caspase 3/7 activity, which is a key player in apoptosis,³⁰ and we found that the apoptotic cell death increased 1.64-fold in CHOL1 cells and 1.32-fold in TFK-1 cells upon treatment with the *FADS2* inhibitor compared with the control (Figure 3B and Figure S1A).

Ferroptosis is another form of programmed cell death, characterized by intracellular iron accumulation and lipid peroxidation, and previous studies identified glutathione peroxidase 4 (GPX4) as an essential regulator of this process.³¹ Given the crucial role of GPX4 in ferroptosis, we evaluated its expression level in relation to CCA tumorigenicity. Treatment with the *FADS2* inhibitor or siFADS2s decreased GPX4 protein expression in both cell lines (Figure 3C and Figure S1B). To confirm this, we measured the GSH/GSSG ratio, which is a marker of ferroptosis.³² Using a GSH assay, inhibition of *FADS2* led to a reduction in the GSH/GSSG ratio by approximately 50.9% in CHOL1 cells and 24.4% in TFK-1 cells compared with the DMSO controls (Figure 3D). These findings suggest that *FADS2* inhibition attenuates GPX4 expression and activity in CCA.

3.4 | Triglyceride alteration in FADS2-depleted cells

FADS2 is a delta-6 desaturase. We hence measured the saturated and unsaturated FA levels by GC-MS. Both FAs were not significantly changed between *FADS2*-depleted cells and control cells (Figure S2A,B). To investigate whether the composition of lipids other than FAs was altered, we performed a lipidomics assay. The levels of various lipids, including triglycerides and cholesterol esters, were decreased in *FADS2* knockdown cells (Figure 4A,B). To confirm this, we measured the number of lipid droplets, which mainly consist of triglycerides and cholesterol esters, in the cells.³³ The intracellular lipid droplets were stained with Lipi-Green, and the Lipi-Green intensity was measured by flow cytometry. In CHOL1 cells, the number of lipid droplets was reduced by 20.9% by *FADS2* knockdown and by 12.0% by *FADS2* inhibition (Figure 4C). In TFK-1 cells, the number of lipid droplets was reduced by 17.6% following *FADS2* knockdown and by 14.6% following *FADS2* inhibition (Figure 4C). These data suggest that depletion of *FADS2* reduces intracellular lipids, especially triglycerides.

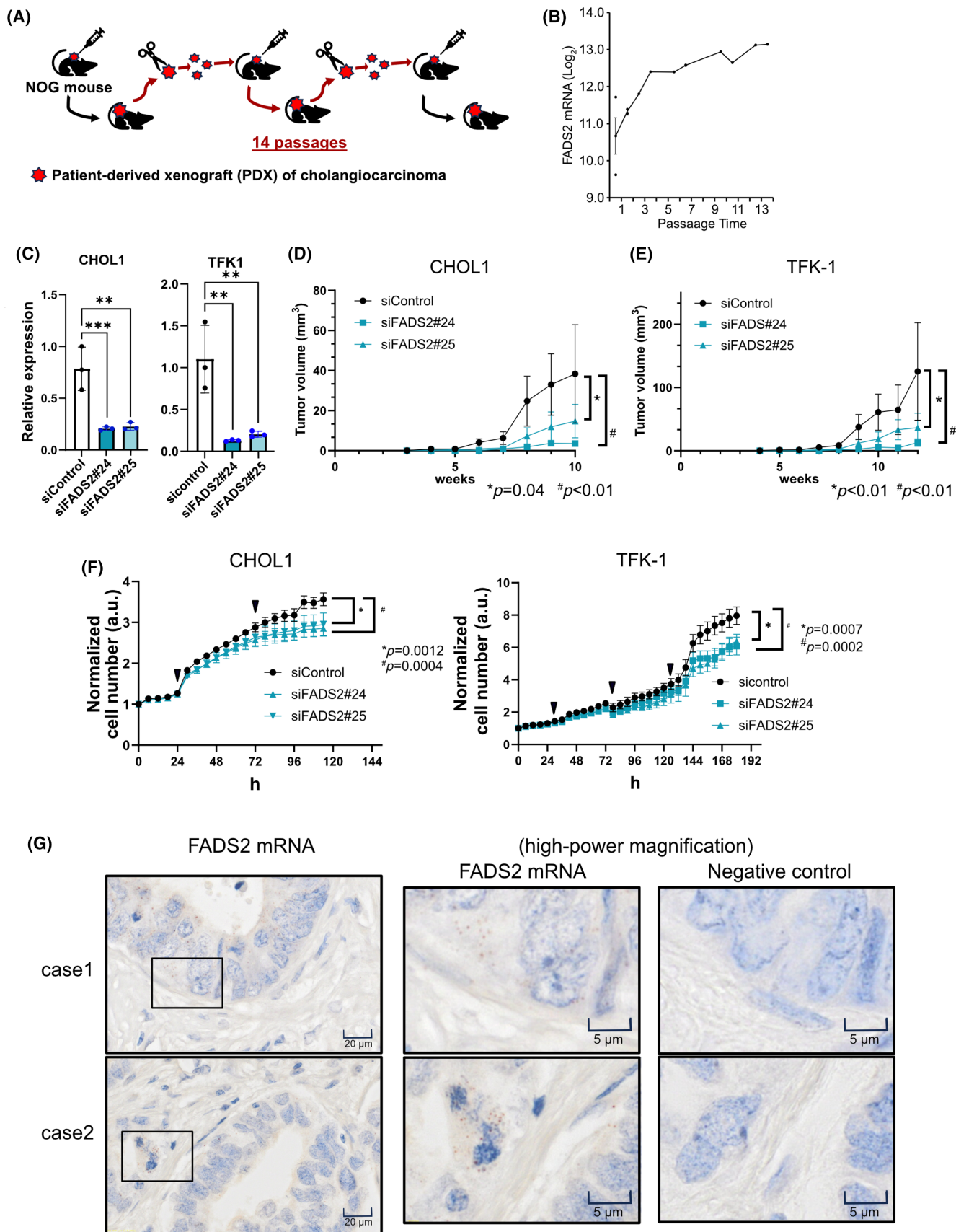


FIGURE 1 Fatty acid desaturase 2 (FADS2) is enriched in serially transplanted xenograft cancer cells (A) Schematic outline of the serially transplanted xenograft model. (B) FADS2 mRNA at each passage point was determined by microarray analysis. (C) FADS2 was knocked down by siRNA, and FADS2 mRNA expression was measured by real-time PCR. $**p < 0.01$, $***p < 0.001$. (D, E) FADS2 knockdown and control cells were transplanted into NOG mice, and the tumor volumes were measured weekly. (D) CHOL1 cells; (E) TFK-1 cells. p -Values were calculated by comparing the nonlinear regression curves of the two groups. (F) Cell proliferation was measured after treatment with siFADS2 using an Incucyte system. Arrowheads indicate the treatment of siRNA. (G) Representative images of FADS2 mRNA expression in cholangiocarcinoma tissues based on RNAscope assay. FADS2 positive appeared as brown spots. Bar (low-magnification images), 20 μ m. Bar (high-magnification images), 5 μ m.

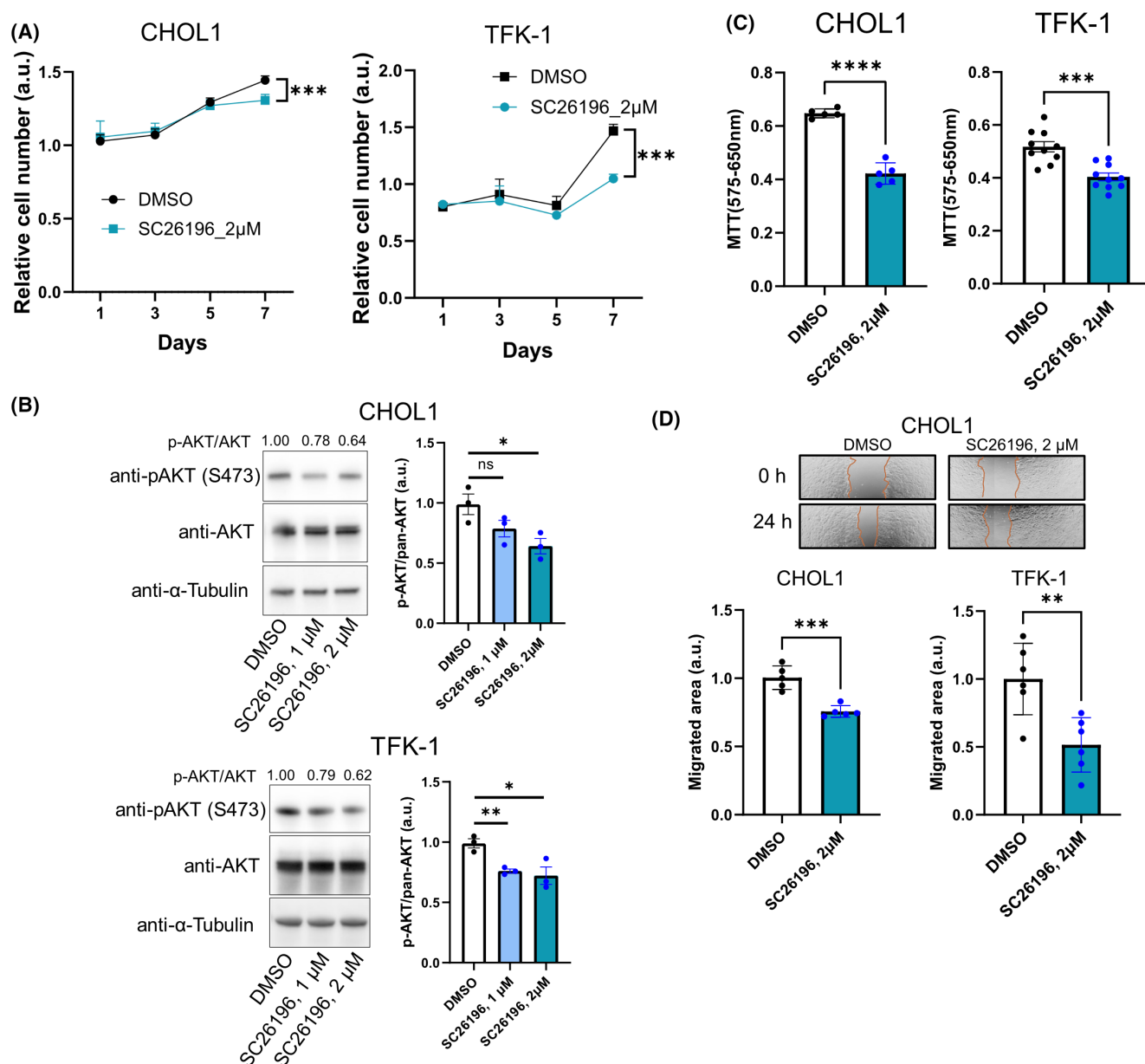


FIGURE 2 Fatty acid desaturase 2 (FADS2) depletion reduces cell proliferation activity. (A) Cell proliferation was measured after treatment with FADS2 inhibitor SC26196 using MTT assay. (B) Western blotting. CHOL1 and TFK-1 cells were harvested at 9 and 4 days after SC26196 addition, respectively. The values indicate the band densities quantified using ImageJ software. (C) Sphere formation assay with SC26196 in CHOL1 and TFK-1 cells using MTT assay. (D) Scratch-wound assay. The migrated areas were measured after 24 h with or without SC26196 treatment. The wound-healing size was quantified using ImageJ software and is shown in the bar graphs. $*p < 0.05$, $**p < 0.01$, $***p < 0.001$, $****p < 0.0001$.

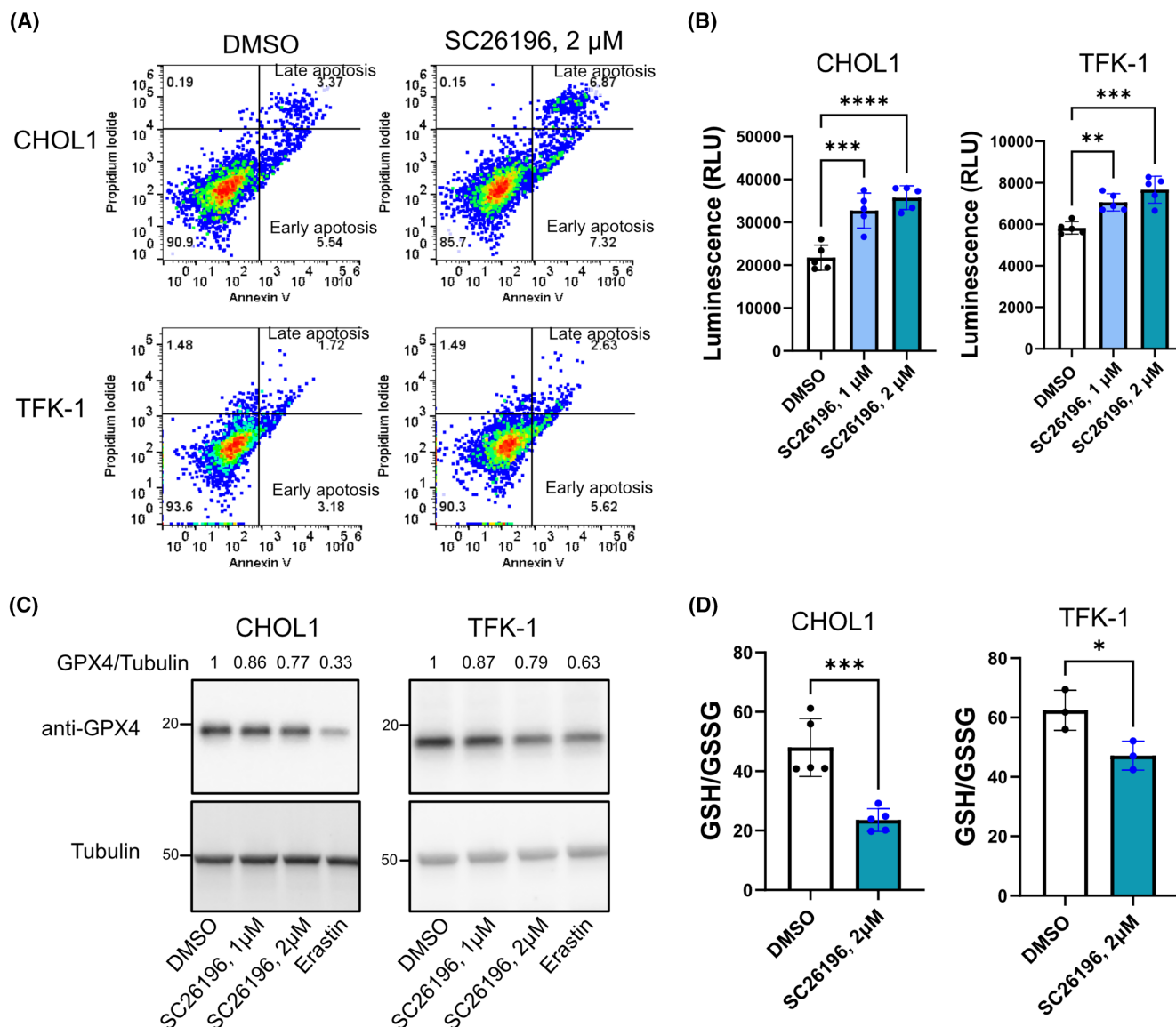


FIGURE 3 Fatty acid desaturase 2 (FADS2) inhibitor alters characteristics of cancer cells. (A) Apoptotic cells were counted by flow cytometry. Apoptotic cells were detected by propidium iodide and/or annexin V-positive staining. (B) Apoptosis assay. Caspase 3/7 activity was measured with a luminometer. (C) Western blotting. Cells were treated with FADS2 inhibitor or erastin (a ferroptosis inducer) for 3 days, and GPX4 protein expression was determined by Western blotting. The values indicate the band densities quantified using ImageJ software. (D) The GSH/GSSG ratio was measured. * $p < 0.05$, ** $p < 0.01$, *** $p < 0.001$, **** $p < 0.0001$.

3.5 | FADS2 inhibition reduced mitochondrial oxygen consumption ratio in CCA

Fatty acids are released from triglycerides by lipase, and mitochondrial FA β -oxidation is a major pathway fueling the tricarboxylic acid cycle.³⁴ To test whether FADS2 depletion alters the β -oxidation pathway, we measured the mitochondrial oxygen consumption ratio. We found that basal and maximal respiration in CHOL1 and TFK-1 cells was decreased by FADS2 inhibition (Figure 4D). Microarray analysis demonstrated that oxidative phosphorylation pathway was negatively correlated with FADS2-depleted cells (Figure S2C). These data suggested that the β -oxidation pathway is attenuated by FADS2 inhibition.

4 | DISCUSSION

FADS2 is a desaturase that plays an important role in polyunsaturated FA synthesis.³⁵ Recently, however, other roles of FADS2 have been reported. In adipocytes, FADS2 deficiency promotes TG lipolysis, resulting in a decrease in lipid droplets.^{36,37} In mouse liver, ablation of FADS2 increases TG and cholesterol accumulation.³⁸ SCD1 is an enzyme that catalyzes the synthesis of monounsaturated fatty acids (MUFAs), but it is also known to affect lipid pathways other than desaturation, such as FA uptake, lipogenesis, and β -oxidation.³⁹ We found that FADS2 knockdown or inhibition did not alter the ratio of unsaturated FAs but significantly reduced the total lipids including triglycerides and cholesterol esters. Our data also demonstrated that the oxygen

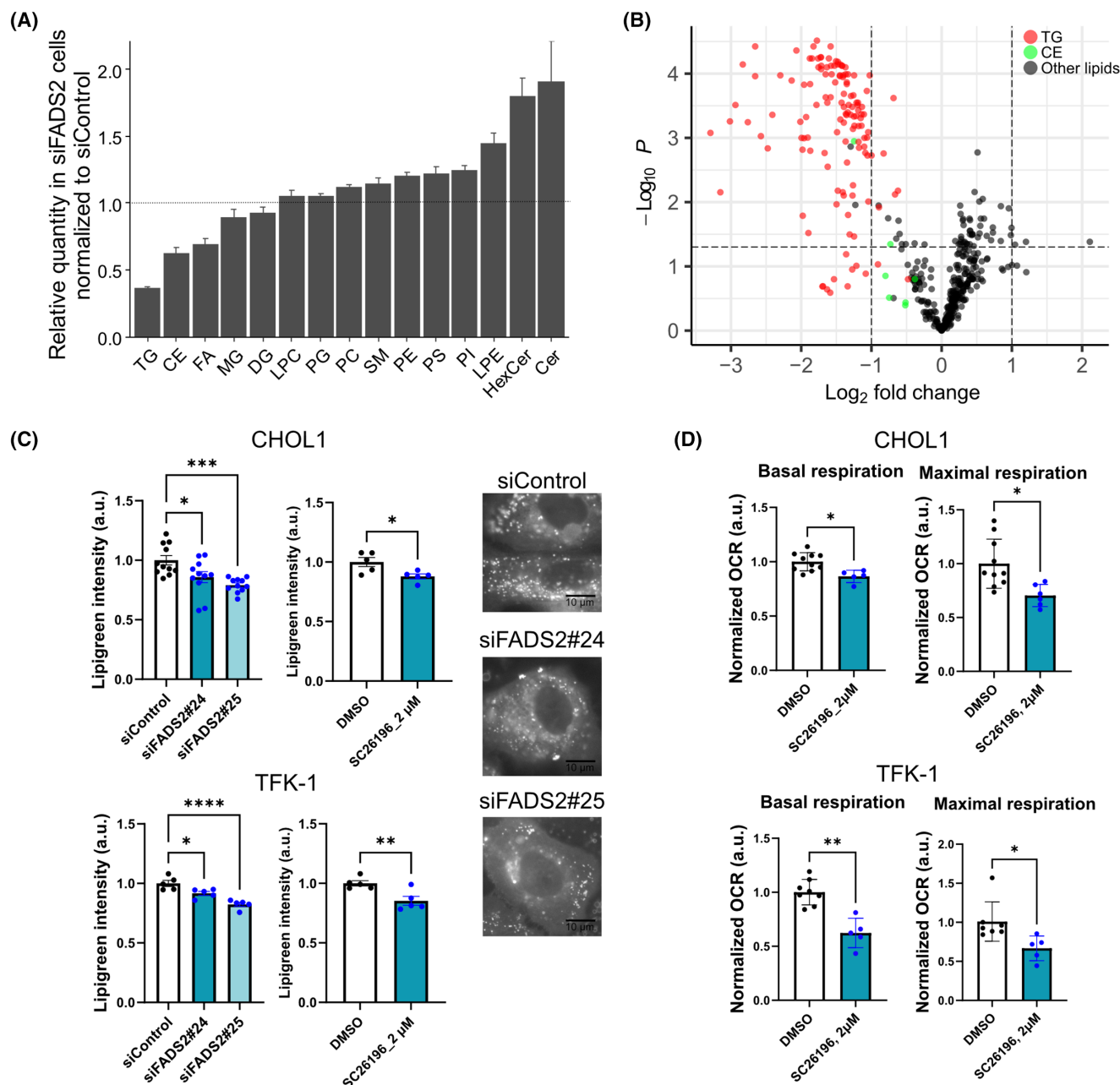


FIGURE 4 Triglyceride is altered in fatty acid desaturase 2 (FADS2)-depleted cells. (A) Lipidomics in FADS2 knockdown CHOL1 cells. Lipids were quantitatively identified by supercritical fluid chromatography–tandem mass spectrometry (SFC-MS/MS) spectrometry and the relative expression of siFADS2s ($n=9$) to siControl ($n=3$) was calculated. TG, triglycerides; CE, cholesterol esters; FA, free fatty acids; MG, monoglycerides; DG, diglycerides; LPC, lysophosphatidylcholine; PG, phosphatidylglycerol; PC, phosphatidylcholines; SM, sphingomyelin; PE, phosphatidylethanolamine; PS, phosphatidylserine; PI, phosphatidylinositol; LPE, lysophosphatidylethanolamine; HexCer, hexosylceramine; Cer, ceramide. (B) Volcano plot. Fold change was calculated based on the values of siFADS2 to siControl samples. Triglycerides are marked with red circles, and the others are gray. (C) CHOL1 and TFK-1 cells were stained by Lipi-Green, and the intensity was measured by flow cytometry. Representative images of CHOL1 cells are shown (scale bar = 10 μm). (D) The oxygen consumption ratio was measured with a flux analyzer. * $p < 0.05$, ** $p < 0.01$, *** $p < 0.001$, **** $p < 0.0001$.

consumption ratio was decreased in FADS2-depleted cells, suggesting that β -oxidation and ATP production are also decreased.⁴⁰ Collectively, FADS2 depletion reduced lipid storage and energy production, resulting in the attenuation of cancer malignancy by reduction of cell proliferation and migration. Although precise mechanisms are still unknown, FADS2 might have a function other than desaturase.

FADS2 is a desaturase enzyme and synthesizes unsaturated FAs, such as $\omega 3$, $\omega 6$, and $\omega 9$. However, in this study, we found no alteration in the amount of unsaturated FAs (Figure S2A,B). Because many biochemical systems including FA synthesis have functional redundancy,⁴¹ other desaturases could recover the pathway in CCA cells. Another possibility is the involvement of a subtle amount of

metabolites which are produced by FADS2 but could not be detected in this study and could act as a ligand for the nuclear receptor.⁴² In this study, membrane fluidity was reduced in FADS2-depleted cells (Figure S2D). Membrane fluidity is controlled by the lipid composition in membranes, and unsaturated FAs contribute to a greater disorder of membranes than saturated FAs at equal absolute temperatures.⁴³ In glioma stem cells, knockdown of ELOVL2, a key enzyme in the synthesis of long polyunsaturated FAs, reduced membrane fluidity.¹³ In this study, saturated/unsaturated FAs in total cell lysates showed no alteration; nonetheless, it is possible that the proportion of unsaturated FAs located in plasma membrane was altered in FADS2-depleted cells.

We demonstrated that FADS2 depletion reduced the content of triglyceride and cholesterol ester, but how FADS2 is involved in the lipid storage is still unclear. SCD1 affect FA transport proteins, resulting in the decrease of TG in the heart.³⁹ It is possible that the uptake of FAs and lipoproteins is reduced in FADS2 depletion cells. Another possibility is that lipid storage is degraded (lipolysis) by autophagy.⁴⁴ Further study is required to identify the new function of FADS2.

In this study, apoptosis and ferroptosis are increased by FADS2 depletion. In ovarian cancer cells, apoptosis and ferroptosis are also increased by SCD1/FADS2 inhibitors.¹² SCD1/FADS2 inhibitors reduced GPX4 expression and increased reactive oxygen species and lipid peroxidation, resulting in ferroptosis.³² We also demonstrated the reduction of GPX4 expression, but total cellular and mitochondrial ROS were not altered by FADS2 inhibition (Figure S3). Previous studies showed that SCD1 contributes to resistance to ferroptosis by producing MUFAs,^{45,46} but our data showed that FADS2 depletion did not alter the FA composition. Therefore, FADS2 might regulate the ferroptosis via unknown mechanisms. Recent studies demonstrated that FADS2 protein interacts with proteins such as STING, ACSL, and SLC27A2.^{47,48} The FADS2-protein complex may play a novel role and further studies are needed to elucidate the mechanisms of cell death by FADS2 depletion.

AUTHOR CONTRIBUTIONS

Kohsei Hasegawa: Formal analysis; investigation; validation; visualization; writing – original draft; writing – review and editing. **Haruna Fujimori:** Formal analysis; funding acquisition; investigation; project administration; validation; visualization; writing – original draft; writing – review and editing. **Kohta Nakatani:** Data curation; methodology; software. **Masatomo Takahashi:** Methodology; software. **Yoshihiro Izumi:** Data curation; methodology; software. **Takeshi Bamba:** Methodology; software. **Mao Nakamura-Shima:** Funding acquisition; resources. **Rie Shibuya-Takahashi:** Validation. **Mai Mochizuki:** Funding acquisition; writing – original draft. **Yuta Wakui:** Funding acquisition; resources. **Makoto Abue:** Resources. **Wataru Iwai:** Resources. **Daisuke Fukushi:** Resources. **Kennichi Satoh:** Funding acquisition; resources. **Kazunori Yamaguchi:** Funding acquisition; writing – original draft. **Norihisa Shindo:** Funding acquisition; writing – original draft. **Jun Yasuda:** Funding acquisition; writing – original draft. **Naoki Asano:** Writing – review and editing.

Takayuki Imai: Resources. **Yukinori Asada:** Resources. **Yukio Katori:** Resources. **Keiichi Tamai:** Conceptualization; formal analysis; funding acquisition; investigation; project administration; supervision; validation; visualization; writing – original draft; writing – review and editing.

ACKNOWLEDGMENTS

This study was supported in part by the Biomedical Research Core of the Tohoku University Graduate School of Medicine.

FUNDING INFORMATION

This study was supported by JSPS KAKENHI (grant no. JP:22K09696, 22K09678, 22K08085, 22K07974, 21K07137, 21K07973, 21K07186, 21H02396, 20K09701, and 19K08430), the Takeda Medical Foundation, the Kobayashi Foundation for Cancer Research, and AMED-BINDS (JP22ama121055 for T.B.) from the Japan Agency for Medical Research and Development (AMED). This work was also partly performed in the MEXT Cooperative Research Project Program, Medical Research Center Initiative for High Depth Omics, and CURE: JPMXP1323015486.

CONFLICT OF INTEREST STATEMENT

The authors declare no conflict of interest.

ETHICS STATEMENT

Approval of the research protocol by an Institutional Reviewer Board: Yes (approval number: 2018-010).

Informed Consent: Cholangiocarcinoma tissues were obtained from the Tohoku University Hospital (Sendai, Japan) with written informed consent.

Registry and the Registration No. of the study/trial: NA.

Animal Studies: Approved by the Miyagi Cancer Center Animal Care and Use Committee (approval number: AE.22.01).

ORCID

Haruna Fujimori  <https://orcid.org/0009-0008-8855-1216>

Keiichi Tamai  <https://orcid.org/0000-0003-0813-5885>

REFERENCES

1. Rizvi S, Khan SA, Hallemeier CL, Kelley RK, Gores GJ. Cholangiocarcinoma—evolving concepts and therapeutic strategies. *Nat Rev Clin Oncol*. 2018;15(2):95-111.
2. Banales JM, Cardinale V, Carpino G, et al. Expert consensus document: Cholangiocarcinoma: current knowledge and future perspectives consensus statement from the European network for the study of Cholangiocarcinoma (ENS-CCA). *Nat Rev Gastroenterol Hepatol*. 2016;13(5):261-280.
3. Bertuccio P, Malvezzi M, Carioli G, et al. Global trends in mortality from intrahepatic and extrahepatic cholangiocarcinoma. *J Hepatol*. 2019;71(1):104-114.
4. Kreso A, Dick JE. Evolution of the cancer stem cell model. *Cell Stem Cell*. 2014;14(3):275-291.
5. Afify SM, Seno M. Conversion of stem cells to cancer stem cells: undercurrent of cancer initiation. *Cancer*. 2019;11(3):345.
6. Anderson NM, Simon MC. The tumor microenvironment. *Curr Biol*. 2020;30(16):921-925.

7. Fujii E, Suzuki M, Matsubara K, et al. Establishment and characterization of in vivo human tumor models in the NOD/SCID/gamma(c) (null) mouse. *Pathol Int*. 2008;58(9):559-567.
8. Brown KM, Xue A, Mittal A, Samra JS, Smith R, Hugh TJ. Patient-derived xenograft models of colorectal cancer in pre-clinical research: a systematic review. *Oncotarget*. 2016;7(40):66212-66225. Accessed October,13. <https://www.ncbi.nlm.nih.gov/pmc/articles/PMC5323228/>
9. Kobayashi S, Yamada-Okabe H, Suzuki M, et al. LGR5-positive colon cancer stem cells interconvert with drug-resistant LGR5-negative cells and are capable of tumor reconstitution. *Stem Cells*. 2012;30(12):2631-2644.
10. Currie E, Schulze A, Zechner R, Walther TC, Farese RV. Cellular fatty acid metabolism and cancer. *Cell Metab*. 2013;18(2):153-161.
11. Li J, Condello S, Thomes-Pepin J, et al. Lipid desaturation is a metabolic marker and therapeutic target of ovarian cancer stem cells. *Cell Stem Cell*. 2017;20(3):303-314.
12. Xuan Y, Wang H, Yung MM, et al. SCD1/FADS2 fatty acid desaturases equipose lipid metabolic activity and redox-driven ferroptosis in ascites-derived ovarian cancer cells. *Theranostics*. 2022;12(7):3534-3552.
13. Gimble RC, Kidwell RL, Kim LJY, et al. Glioma stem cell-specific Superenhancer promotes polyunsaturated fatty-acid synthesis to support EGFR signaling. *Cancer Discov*. 2019;9(9):1248-1267.
14. Imai T, Tamai K, Oizumi S, et al. CD271 defines a stem cell-like population in hypopharyngeal cancer. *PLoS One*. 2013;8(4):e62002.
15. Yasumoto A, Fujimori H, Mochizuki M, et al. BEX2 is poor prognostic factor and required for cancer stemness in gastric cancer. *Biochem Biophys Res Commun*. 2023. Accessed March, 16. <https://www.sciencedirect.com/science/article/pii/S0006291X23003029>;655:59-67.
16. Tamai K, Nakamura-Shima M, Shibuya-Takahashi R, et al. BEX2 suppresses mitochondrial activity and is required for dormant cancer stem cell maintenance in intrahepatic cholangiocarcinoma. *Sci Rep*. 2020;10(1):21592. doi:10.1038/s41598-020-78539-0
17. Fukushi D, Shibuya-Takahashi R, Mochizuki M, et al. BEX2 is required for maintaining dormant cancer stem cell in hepatocellular carcinoma. *Cancer Sci*. 2021;112:4580-4592.
18. Katayama H, Tamai K, Shibuya R, et al. Long non-coding RNA HOTAIR promotes cell migration by upregulating insulin growth factor-binding protein 2 in renal cell carcinoma. *Sci Rep*. 2017;7(1):12016.
19. R Core Team. R: A Language and Environment for Statistical Computing. R Foundation for Statistical Computing; 2019. <https://www.R-project.org/>
20. Subramanian A, Tamayo P, Mootha VK, et al. Gene set enrichment analysis: a knowledge-based approach for interpreting genome-wide expression profiles. *Proc Natl Acad Sci USA*. 2005;102(43):15545-15550.
21. Nueda MJ, Tarazona S, Conesa A. Next maSigPro: updating maSigPro bioconductor package for RNA-seq time series. *Bioinformatics*. 2014;30(18):2598-2602.
22. Corenblum M, McRobbie-Johnson A, Carruth E, et al. Parallel neurodegenerative phenotypes in sporadic parkinson's disease fibroblasts and midbrain dopamine neurons. *Prog Neurobiol*. 2023;229:102501.
23. Bligh EG, Dyer WJ. A rapid method of total lipid extraction and purification. *Can J Biochem Physiol*. 1959;37(8):911-917.
24. Fushimi T, Izumi Y, Takahashi M, Hata K, Murano Y, Bamba T. Dynamic metabolome analysis reveals the metabolic fate of medium-chain fatty acids in AML12 cells. *J Agric Food Chem*. 2020;68(43):11997-12010.
25. Takeda H, Izumi Y, Takahashi M, et al. Widely-targeted quantitative lipidomics method by supercritical fluid chromatography triple quadrupole mass spectrometry. *J Lipid Res*. 2018;59(7):1283-1293.
26. Harmon SD, Kaduce TL, Manuel TD, Spector AA. Effect of the delta6-desaturase inhibitor SC-26196 on PUFA metabolism in human cells. *Lipids*. 2003;38(4):469-476.
27. Revathidevi S, Munirajan AK. Akt in cancer: mediator and more. *Semin Cancer Biol*. 2019;59:80-91.
28. Ishiguro T, Ohata H, Sato A, Yamawaki K, Enomoto T, Okamoto K. Tumor-derived spheroids: relevance to cancer stem cells and clinical applications. *Cancer Sci*. 2017;108(3):283-289.
29. Hanahan D. Hallmarks of cancer: new dimensions. *Cancer Discov*. 2022;12(1):31-46.
30. McIlwain DR, Berger T, Mak TW. Caspase functions in cell death and disease. *Cold Spring Harb Perspect Biol*. 2013;5(4):a008656.
31. Ma T, Du J, Zhang Y, Wang Y, Wang B, Zhang T. GPX4-independent ferroptosis—a new strategy in disease's therapy. *Cell Death Dis*. 2022;8(1):434.
32. Ursini F, Maiorino M. Lipid peroxidation and ferroptosis: the role of GSH and GPx4. *Free Radic Biol Med*. 2020;152:175-185.
33. Zhang C, Liu P. The lipid droplet: a conserved cellular organelle. *Protein Cell*. 2017;8(11):796-800.
34. Houten SM, Violante S, Ventura FV, Wanders RJA. The biochemistry and physiology of mitochondrial fatty acid β -oxidation and its genetic disorders. *Annu Rev Physiol*. 2016;78:23-44.
35. Glaser C, Heinrich J, Koletzko B. Role of FADS1 and FADS2 polymorphisms in polyunsaturated fatty acid metabolism. *Metabolism*. 2010;59(7):993-999.
36. Wang C, Hucik B, Sarr O, et al. Delta-6 desaturase (Fads2) deficiency alters triacylglycerol/fatty acid cycling in murine white adipose tissue. *J Lipid Res*. 2023;64(6):100376.
37. Wang C, MacIntyre B, Mutch DM. Inhibition of Δ -6 desaturase reduces fatty acid re-esterification in 3T3-L1 adipocytes independent of changes in n3-PUFA cellular content. *Biochim Biophys Acta Mol Cell Biol Lipids*. 2022;1867(7):159160.
38. Hayashi Y, Lee-Okada HC, Nakamura E, et al. Ablation of fatty acid desaturase 2 (FADS2) exacerbates hepatic triacylglycerol and cholesterol accumulation in polyunsaturated fatty acid-depleted mice. *FEBS Lett*. 2021;595(14):1920-1932.
39. Dobrzyn P, Bednarski T, Dobrzyn A. Metabolic reprogramming of the heart through stearoyl-CoA desaturase. *Prog Lipid Res*. 2015;57:1-12.
40. Fukaya M, Sato Y, Kondo S, Adachi SI, Yoshizawa F, Sato Y. Quercetin enhances fatty acid β -oxidation by inducing lipophagy in AML12 hepatocytes. *Heliyon*. 2021;7(6):e07324.
41. Ruppe S, Mains K, Fox JM. A kinetic rationale for functional redundancy in fatty acid biosynthesis. *Proc Natl Acad Sci USA*. 2020;117(38):23557-23564.
42. Sampath H, Ntambi JM. Polyunsaturated fatty acid regulation of gene expression. *Nutr Rev*. 2004;62(9):333-339.
43. Holte LL, Peter SA, Sinnwell TM, Gawrisch K. 2H nuclear magnetic resonance order parameter profiles suggest a change of molecular shape for phosphatidylcholines containing a polyunsaturated acyl chain. *Biophys J*. 1995;68(6):2396-2403.
44. Grabner GF, Xie H, Schweiger M, Zechner R. Lipolysis: cellular mechanisms for lipid mobilization from fat stores. *Nat Metab*. 2021;3(11):1445-1465.
45. Luis G, Godfroid A, Nishiumi S, et al. Tumor resistance to ferroptosis driven by Stearoyl-CoA Desaturase-1 (SCD1) in cancer cells and fatty acid binding Protein-4 (FABP4) in tumor microenvironment promote tumor recurrence. *Redox Biol*. 2021;1(43):102006.
46. Long noncoding RNA LINC01606 protects colon cancer cells from ferroptotic cell death and promotes stemness by SCD1-Wnt/ β -catenin-TFE3 feedback loop signalling—Luo—2022—clinical and translational medicine—wiley online library. 2024. <https://onlinelibrary.wiley.com/doi/full/10.1002/ctm2.752>.
47. Vila IK, Chamma H, Steer A, et al. STING orchestrates the crosstalk between polyunsaturated fatty acid metabolism and inflammatory responses. *Cell Metab*. 2022;34(1):125-139.

48. Chu H, Zhao Q, Liu J, et al. Ionic liquid-based extraction system for in-depth analysis of membrane protein complexes. *Anal Chem*. 2022;94(2):758-767.

SUPPORTING INFORMATION

Additional supporting information can be found online in the Supporting Information section at the end of this article.

How to cite this article: Hasegawa K, Fujimori H, Nakatani K, et al. Delta-6 desaturase FADS2 is a tumor-promoting factor in cholangiocarcinoma. *Cancer Sci*. 2024;115:3346-3357. doi:[10.1111/cas.16306](https://doi.org/10.1111/cas.16306)